Received: 27 March 2018 | Accepted: 28 May 2018

DOI: 10.1111/jace.15805

Journal of the American Ceramic Society

ORIGINAL ARTICLE

Amorphous zirconia at high pressure

Murat Durandurdu

Department of Materials Science & Nanotechnology Engineering, Abdullah Gül University, Kayseri, Turkey

Correspondence
Murat Durandurdu, Department of Materials Science & Nanotechnology Engineering, Abdullah Gül University, Kayseri, Turkey.
Email: murat.durandurdu@agu.edu.tr

Funding information
Abdullah Gül University Support Foundation

Abstract

We show, by means of ab initio calculations, that amorphous zirconia progressively transforms to a high-density amorphous phase with the application of pressure. The average coordination number of Zr and O atoms under pressure rises gradually to 8 and 4, respectively. The main building unit of the dense noncrystalline state is the eightfold-coordinated Zr atoms (62.5%). When the coordinated modification of Zr atoms in the zirconia crystal at high pressure and temperature conditions is considered, it can be perceived that amorphous zirconia follows a transformation mechanism similar to the one observed at high temperature but different than the one detected at high pressure. The dense disordered phase is indeed found to be locally comparable with the high-temperature tetragonal crystal. Upon decompression, some high-pressure arrangements are persevered in the model and a transformation into another amorphous state whose structure is intermediate between uncompressed and dense amorphous phases is observed in the simulations. The high-pressure amorphous structures are found to be semiconductors with a band gap smaller than that of the original model.

KEYWORDS
amorphous, high pressure, phase transformation, zirconia

1 | INTRODUCTION

Zirconia (ZrO_2) polymorphs have been investigated comprehensively for last decades and their remarkable dielectric, physical, mechanical, electronic, thermal, and biocompatibility properties have been revealed. These superior properties lead to their various high tech applications, for instance, high-temperature solid oxide fuel cell electrolytes,[1–3] microelectronics,[4–6] medical devices,[7] dentistry,[8] catalyst[9] etc.

The ground state structure of ZrO_2 is the monoclinic baddeleyite crystal ($P2_1/c$) with β ~99.4°. The baddeleyite → tetragonal ($P4_2/nmc$) → cubic ($Fm3m$) transformations are observed at 1170 and 2370°C, respectively.[10–13] The tetragonal phase has the distorted eightfold coordination of Zr atoms while the cubic phase has the perfect eightfold coordination of cations. At high pressures, different transformation mechanisms have been proposed for ZrO_2 in experimental and theoretical studies[14–27] to date. Yet the most accepted mechanism is the baddeleyite→*Pbca*→*Pnma* (cotunnite) phase transformations. In the first transformation, no coordination modification around Zr atoms is experienced while in the second one the coordination of Zr atoms increases from 7 to 9.

The amorphous state of ZrO_2 (a-ZrO_2) has various important technological applications as well.[5,28–30] The theoretical investigations based on first-principles molecular dynamics (MD) simulations[31–34] have revealed that it has a local structure analogous to that of the baddeleyite phase. The crystallization behavior of a-ZrO_2 at high temperatures has been also experimentally explored. The picture is, however, not as clear as in the crystal. Depending on the sample properties (preparation techniques) and the temperature applied, a structural phase transformation from a-ZrO_2 to monoclinic, tetragonal (high-temperature form), tetragonal (high-temperature form) + amorphous state, cubic + amorphous state etc. has been reported in various experiments.[35–37] Interestingly, the transformation temperatures

reported for the a-ZrO_2→tetragonal phase change are quite smaller than 1170°C at which point the monoclinic → tetragonal phase transformation occurs. To our knowledge, the response of a-ZrO_2 to high pressures has not been explored in any study so far. Two types of phase transformations can be projected for a-ZrO_2: a transformation to a dense amorphous phase or to a crystalline state. The prediction of a quenchable new crystal structure or a quenchable dense noncrystalline structure with new electric and/or mechanical properties might lead to new applications of ZrO_2 in technology.

The aim of present work is, for the first time, to probe the response of a-ZrO_2 to high pressure using a first principles constant pressure technique. A structural change from a low density amorphous (LDA) phase to a high-density amorphous (HDA) phase is perceived through our simulations. The main local structure of the HDA phase is found to be similar to that of the tetragonal crystal (high-temperature form). Upon decompression, another high-density disordered state is recovered, which has an intermediate structure between LDA and HDA configurations.

2 | METHOD

The ab initio code, SIESTA,[38] was preferred to simulate the high-pressure behavior of a-ZrO_2. The Troulier-Martins pseudopotentials,[39] the generalized gradient approximation[40] and the double-ζ polarized orbitals were selected for the simulations. The parameters (basis, pseudopotentials, etc.) used in this study were found to be good enough to capture high-pressure phases of the ZrO_2 crystal[25,27] and to generate a-ZrO_2.[34] Our amorphous model[34] was created from the liquid state using "melt and quench" technique and it is comparable with the other first-principles MD models.[31–33] Each MD time step was set to 1.0 fs. The model consists of 144 atoms. The isoenthalpic-isobaric ensemble (NPH), constant pressure relaxation, was applied to investigate the pressure-induced phase transformation of a-ZrO_2. In this ensemble the atomic positions and the simulation cell shape and size were optimized. Furthermore during the simulations, we chose the power quenching approach, in which the velocity components for atoms or simulation cell were set to 0 when the velocities and forces had opposite signs. Using this ensemble, in our earlier works, we were able to reproduce or predict amorphous-to-amorphous, amorphous-to-crystal, and crystal-to-crystal phase changes in a wide range of materials. We need to underline here that after full relaxation of a-ZrO_2 using the NPH ensemble, we found some structural rearrangements in the model, which yielded a slightly different coordination distribution than what we had reported in Ref. 34. The external pressure was applied by the Parrinello and Rahman technique[41] and increased an increment of 3-5 GPa. At each applied pressure, the structure was optimized until the force tolerance was smaller than 0.01 eV/Å.

3 | RESULTS

The amorphous model is progressively densified under pressure up to 70 GPa and its equation of state is provided in Figure 1. The volume decreases gradually and shows a small discontinuity at 27 and 45 GPa. These discontinuities might denote a possible first-order like phase transformation in a-ZrO_2 or they might be connected with the small size of the simulation box. Upon pressure release, the original volume is not recovered, which may indicate the occurrence of irretrievable structural changes in a-ZrO_2.

The local structural modification of a-ZrO_2 with the application of pressure is first probed by the partial pair distribution functions (PPDFs) as illustrated in Figure 2. As understood from the figure, the model still represents the typical characteristics of an amorphous network at the highest pressure applied in the present work since it exhibits a strong short-range order but no long-range order. This finding can be inferred as the existence of a pressure-induced amorphous-to-amorphous phase transformation in a-ZrO_2.

In order to see how the system is packed under external pressure, the variation in the Zr–O, Zr–Zr, and O–O distances as a function of pressure is explored and offered in Figure 3. At ambient pressure, the main Zr–O, Zr–Zr, and

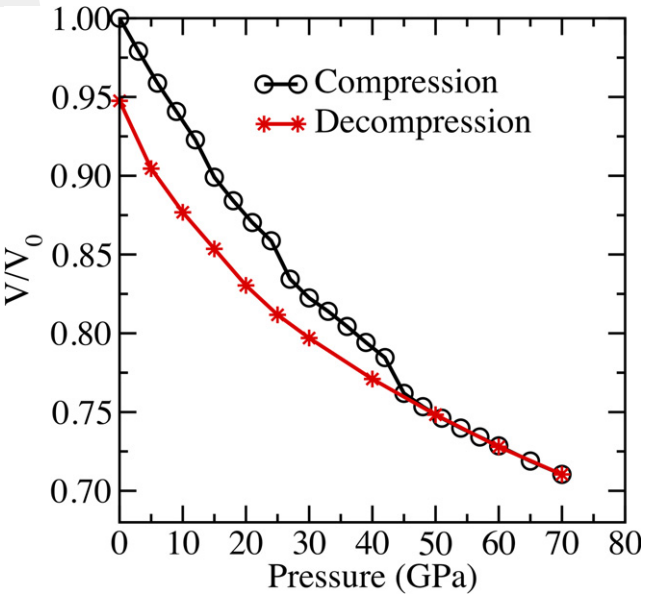

FIGURE 1 Pressure-volume relation of a-ZrO_2 under compression and decompression processes

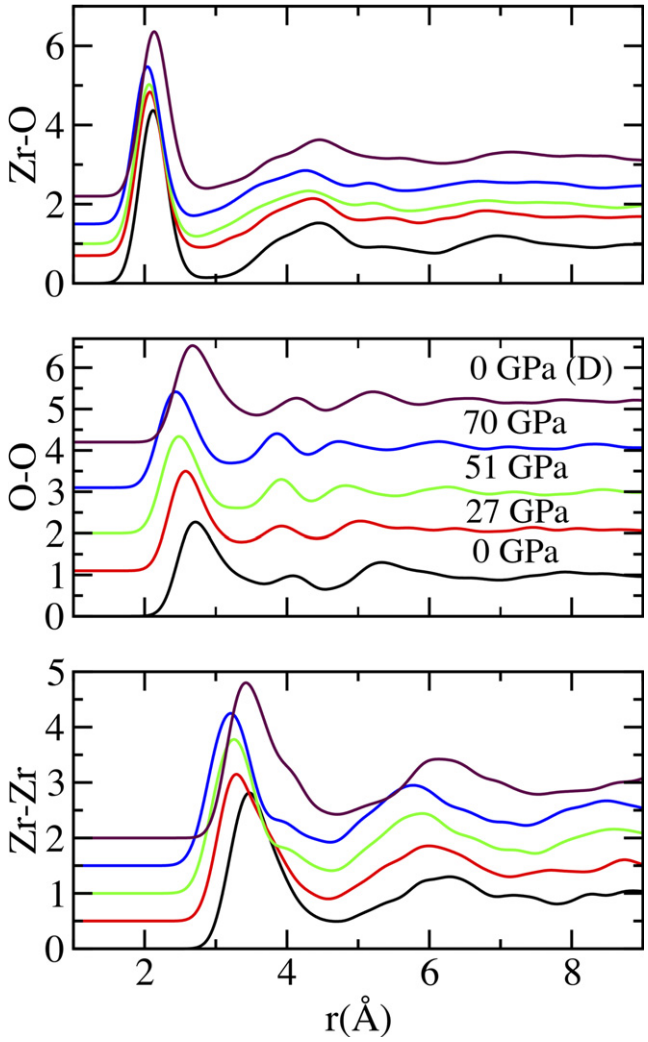

FIGURE 2 Partial pair distribution functions (PPDF) at some pressures. D represents decompression

O–O peaks are located at 2.12, 3.47, and 2.71 Å, respectively and they are parallel to the values of 2.11, 3.50, and 2.80 Å reported for *a*-ZrO_2 in the earlier investigations.[31] For the monoclinic ZrO_2 phase, these peaks appear at ~2.13, 3.44 and 2.74 Å. When the model is subjected to the external pressure, the position of all peaks shift gradually to lower distances. The Zr–O bond length seems to be less sensitive to pressure relative to the other separations. The change in the Zr–O length is smaller than 4%. Both Zr–Zr and O–O separations decline with almost the same degree up to 42 GPa at which point the alteration of the Zr-Zr correlation becomes much slower, which is probably related to the formation of ninefold-coordinated Zr atoms in the model at this pressure and thereafter (see below).

Since most phase transformations are generally identified by the modification of the coordination number, the variation in mean coordination number of Zr and O atoms with increasing external pressure is investigated and given in

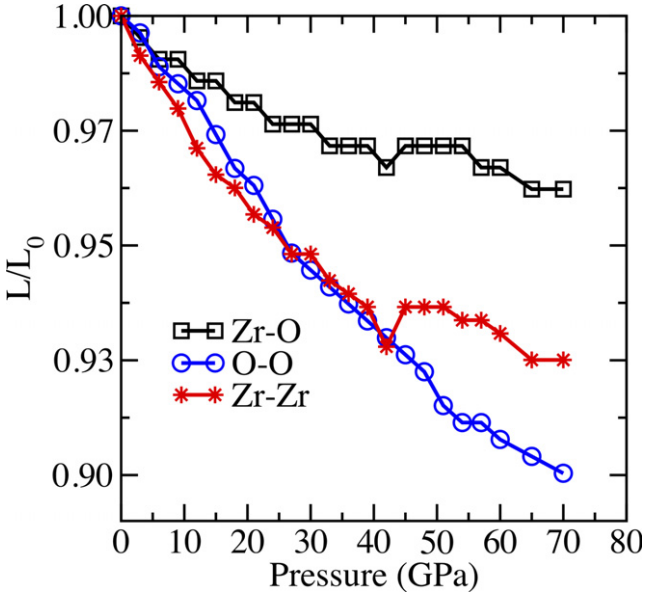

FIGURE 3 Variation in Zr–O, Zr–Zr and O–O distances as a function of pressure. Zr–O, Zr–Zr, and O–O distances are normalized to values of 2.12, 3.47, and 2.71 Å, respectively

Figure 4. The first minimum of Zr–O correlation is used as a cutoff to estimate the partial coordination numbers. At ambient pressure, the average coordination numbers of Zr and O atoms are ~6.81 and ~3.4, respectively. As the external pressure is applied progressively, the mean coordination number begins to increase at 6 GPa, reaches a value of ~8.0 for Zr atoms and of ~4.0 for O atoms at 51 GPa and then they remain almost null up to 70 GPa. This observation reveals that the structural phase transformation occurs in a wide pressure range from 6 to 51 GPa in the simulation and the average coordination number of Zr and O atoms in the HDA phase are about 8.0 and 4.0, respectively. Upon pressure release, the partial coordination numbers slowly decrease and have a value of 7.22 for Zr atoms and of 3.61 for O atoms, which are distinctively higher than those of the uncompressed configuration. This means that some high-pressure formations persist in the network during the pressure release and the dense noncrystalline system converts to another high-density amorphous phase (labeled as a HDA2 phase), which is, as understood, an intermediate state between LDA and HDA structures. This finding denotes that the LDA-to-HDA phase transformation of *a*-ZrO_2 is irreversible.

The coordination distribution illustrated in Figure 5 can provide valuable information about the local structure of *a*-ZrO_2 at different pressures. At ambient condition, Zr atoms have sixfold (~25.5%), sevenfold (~68.75%), and eightfold (~6.25%) configurations while O atoms form twofold (~4%), threefold (~51%), and fourfold (~45%) configurations. As the model is densified under pressure, the number of sixfold coordination declines slowly and

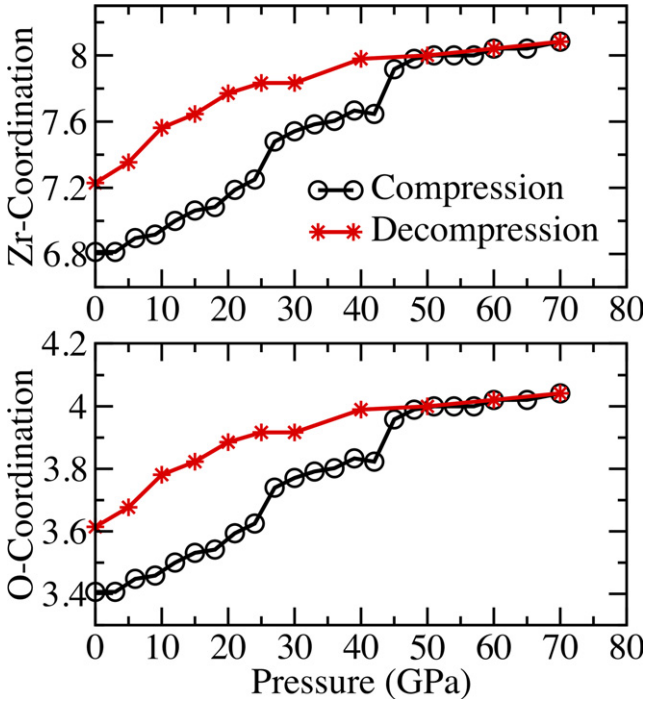

FIGURE 4 Modification of the mean coordination number of Zr and O atoms under pressure

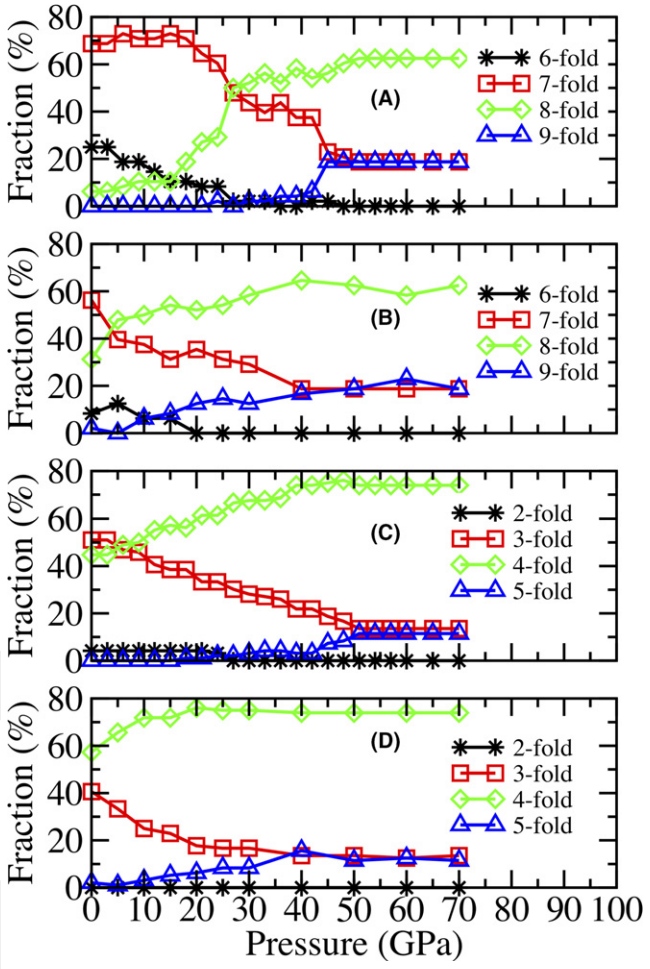

FIGURE 5 The coordination distribution of Zr and O atoms as a function of pressure. A, Zr atoms on compression (B) Zr atoms on decompression (C) O atoms on compression and (D) O atoms on decompression

becomes negligibly small after 24 GPa. On the other hand, the sevenfold and eightfold-coordinated configurations present a drastic change beyond 15 GPa: the amount of the sevenfold-coordinated Zr atoms declines progressively and the parallel to this decrease the fraction of eightfold ones rises. After 51 GPa, both reach a constant value. The ninefold-coordinated clusters appear first at 30 GPa and severely increase between 42 and 51 GPa. At 51 GPa and thereafter, the fraction of sevenfold, eightfold and ninefold-coordinated unites are ~18.75%, ~62.5% and ~18.75%, respectively. When the O atoms are concerned, as expected, the external pressure leads to the formation of more fourfold and even fivefold (between 41 and 51 GPa) configurations. The HDA phase at 51 GPa consists of threefold (~13.6%), fourfold (~74%), and fivefold (~11.5%)-coordinated O atoms. On decompression, the percentage of the high-pressure arrangements decreases and at zero-pressure the HDA2 structure has sixfold (~8.33%), sevenfold (~56.25%), and eightfold (~31.25%)-coordinated Zr atoms and threefold (~40.6%), fourfold (~57.3%), and fivefold (~2.1%)-coordinated O atoms. When the HDA2 structure is compared with the original network (LDA), one can see that some high-pressure structures, in particular, the eightfold-coordinated Zr atoms persist in the amorphous configuration and hence the decompressed model is partially different from the original one. It should be noted here that the ninefold-coordinated motifs (cotunnite-like see below) do not persevere during the decompression process; this is different from our expectation because the cotunnite phase of ZrO_2 is actually quenchable to ambient condition.

In order to get additional knowledge about the short-range order of a-ZrO_2 and its modification at high pressures, we explore bond angle distribution functions and demonstrate them in Figure 6. The zero-pressure LDA model exhibits a broad distribution: the Zr–O–Zr angles range from 70 to 170° and have 2 main peaks at ~98 and 105° while the O–Zr–O angles vary from 45 to 180° with a main peak at ~75°. For the monoclinic phase, the Zr–O–Zr angles are located near 102, 109, 133, and 147°, and the O–Zr–O angles are at around 75, 88, 100, 117, 132, 140, 146, 156, and 168°. Note that the main peaks of the monoclinic crystal at 102-109 and 75° are well captured in the LDA model and hence they structurally resemble each other. When the applied pressure is increased, the general shape of the angle distributions does not change radically and only main peaks somewhat shift to lower angles. Since

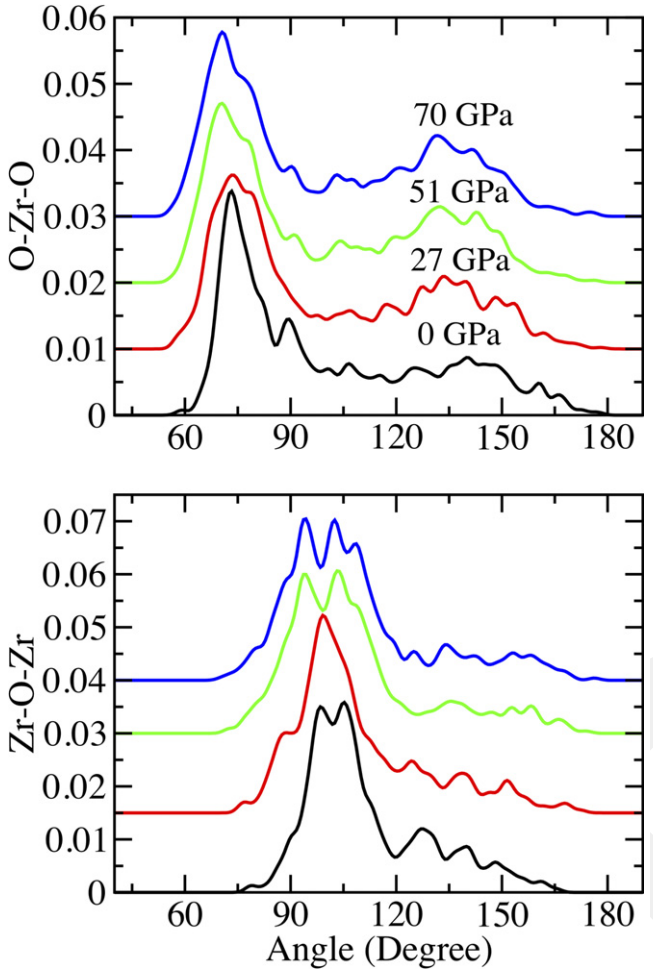

FIGURE 6 Bond angle distribution functions at selected pressures

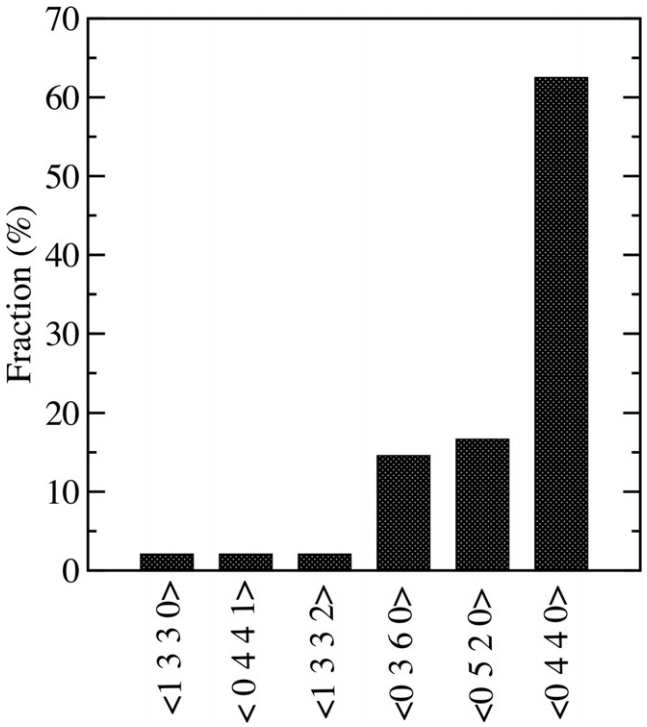

FIGURE 7 Fraction of Zr centered Voronoi polyhedrons at 51 GPa

the key-building units of the HDA structure are the eightfold-coordinated Zr atoms, we can compare the HDA phase with the eightfold-coordinated high-temperature cubic and tetragonal structures. The cubic crystal has the O–Zr–O peaks at 70 and 110° with the same magnitude and a weak O–Zr–O peak near 180° and a strong Zr–O–Zr peak at 110°. In the HDA phase, the lack of pronounced peak at 110 and 180° indicates that there is no resemblance between these structures. On the other hand, the tetragonal phase having the distorted eightfold coordination of Zr atoms, high-temperature form, has the Zr–O–Zr angles at ~96, 108 (pronounced) and 120° and the O–Zr–O angles at ~70 (pronounced), 96, 103, 115, 120 and 167°. Therefore one can see that the local structural arrangement of the HDA phase is quite similar to that of the tetragonal crystal. This suggestion is further supported by the Voronoi polyhedra analysis.[42] According to the analysis, at 51 GPa and thereafter the HDA phase predominantly consists of the Voronoi polyhedrons with the indices of <0 5 2 0> (17%), <0 3 6 0> (15%) and <0 4 4 0> (62.5%) for Zr atoms (see Figures 7 and 8). Here it should be noted that the indices <0 3 6 0> and <0 4 4 0> are two of the leading building units of the cotunnite and tetragonal crystals, respectively. So one can see that the HDA state carries the signature of the cotunnite and tetragonal crystals.

We lastly investigate the effect of the external pressure on the electronic structure of *a*-ZrO_2 by calculating electron density of states and focusing on the variation in the HOMO-LUMO band gap energy under hydrostatic pressure as shown in Figure 9. The band gap energy of the *a*-ZrO_2 model is about 3.5 eV, comparable with the previous simulation estimations of 2.7-3.4 eV[31,32] but as anticipated, it is considerably smaller than the experimental value of 4.7-5.1 eV[37,43] due to the self-interaction error in (DFT)-GGA calculations. With the application of pressure, the HOMO-LUMO band gap decreases. Yet the change in the band gap energy between 42 and 51 GPa is too drastic which is probably related to a significant increase in the number of ninefold-coordinated Zr atoms. On decompression, the band gap energy increases and reaches a value of 3.0 eV at zero pressure. This finding indicates a correlation between the coordination number and band gap energy in *a*-ZrO_2.

4 | DISCUSSION

Because the coordination number alteration takes place in a wide pressure range from 6 to 51 GPa in *a*-ZrO_2, we conclude that the LDA-to-HDA phase change is a gradual

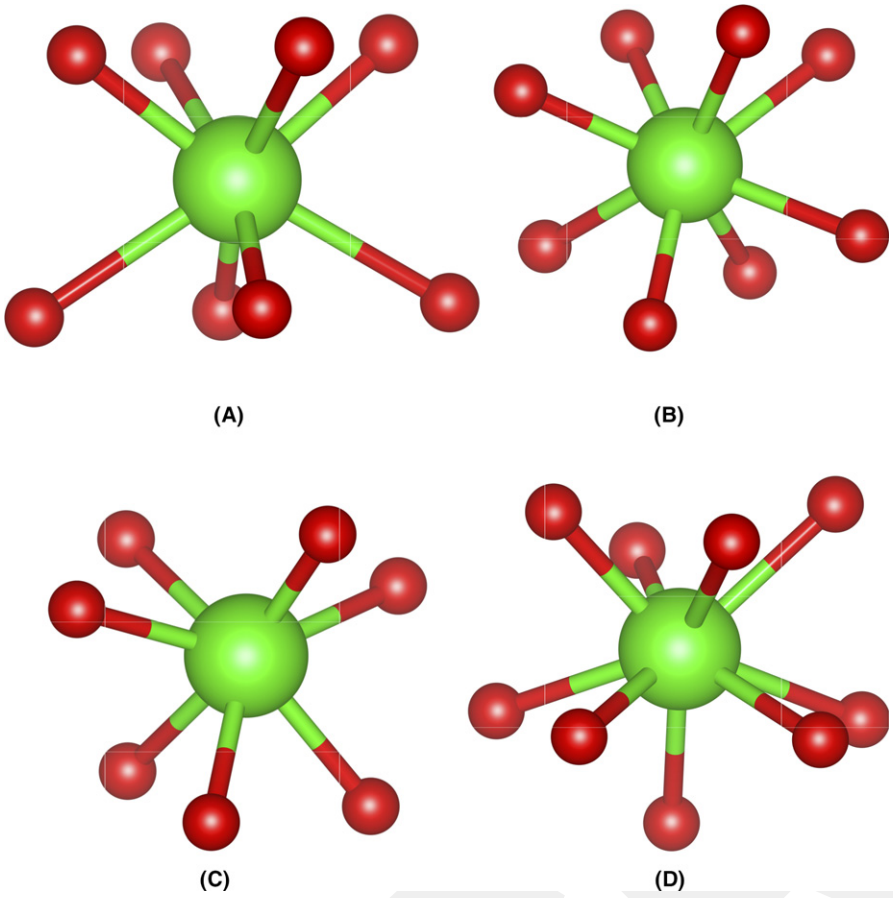

FIGURE 8 Ball stick representation of Zr centered Voronoi polyhedrons (A) the main building unit of the tetragonal phase (the unit has the index of <0 4 4 0>), (B) eightfold-coordinated polyhedron with the index of <0 4 4 0> formed in *a*-ZrO_2, (C) sevenfold-coordinated polyhedron with the index of < 0 5 2 0> structured in *a*-ZrO_2 and (D) ninefold-coordinated polyhedron with the index of <0 3 6 0> formed in *a*-ZrO_2. Large and small spheres are Zr and O atoms, respectively

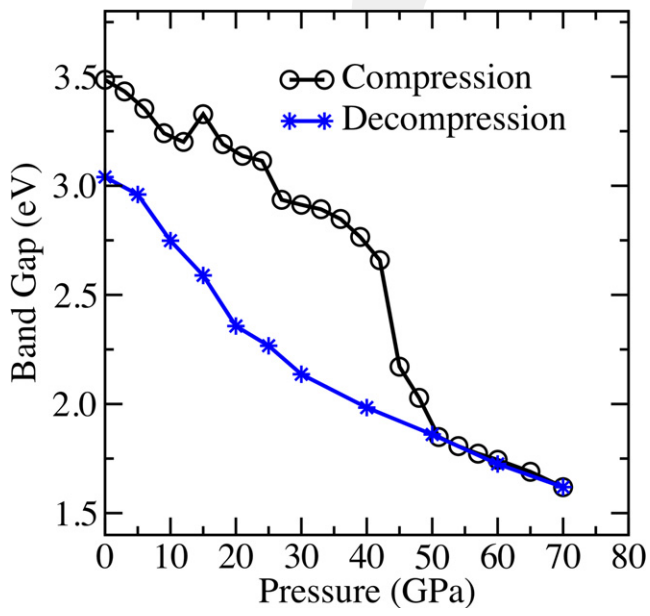

FIGURE 9 Variation in HOMO-LUMO band gap energy under pressure

phase transformation and the small discontinues presented in the pressure-volume relation are a finite size artifact. Of course this can be clarified by experiments and additional theoretical investigations considering large simulation cells. Upon pressure release, the original amorphous network is not fully recovered and a transformation into another amorphous state (HDA2) is obtained. Thus the pressure-induced phase transformation of *a*-ZrO_2 is classified as an irreversible phase transformation. Yet we need to point out here that ab initio MD simulations use a rather short time scale, indicating a fast compression or decompression rate, relative to experiments. So one might think that the fast pressurizing/depressurizing rate is responsible for this irreversible amorphous-to-amorphous phase transformation since the fast pressurizing/depressurizing rate might not allow enough time for the structural relaxation or arrangement to take place, producing frozen states. Of course such a scenario is possible but we need to underline here that using the same simulation technique, in spite of the fast compression or decompression rate, in our earlier works, we have successfully reproduced experimentally proposed reversible/irreversible amorphous-to-amorphous, amorphous-to-crystal, crystal-to-crystal phase transformations in a wide range of materials. Nonetheless, additional studies, in particular, experimental ones, are surely desirable to clarify this issue.

In the noncrystalline state of ZrO_2, the transformation involves a coordination change from about 6.81-8. So one

can see that this mechanism is different from that of the ZrO_2 crystal because in the crystal the mechanism engages with the coordination modifications of 7→7→9 with increasing pressure. On the other hand, this mechanism is similar to what has been witnessed in ZrO_2 at high temperature because the HDA phase principally consists of eightfold-coordinated Zr atoms and its short-range arrangement is mostly similar to the main building unit of the tetragonal phase.

The persistent of the tetragonal-like eightfold-coordinated Zr atoms during decompression is particularly important because the decompressed HDA2 phase can have a higher dielectric constant than *a*-ZrO_2 since the tetragonal phase presents the largest dielectric constant.[33] Based on our findings, here we will speculate that if *a*-ZrO_2 is prepared under some pressure conditions, more tetragonal-like configurations can be provoked in *a*-ZrO_2 and hence its dielectric properties can be improved.

The formation of ninefold-coordinated cotunnite-like structures might suggest that a phase transformation from the HDA phase to the cotunnite-like very high-density amorphous (VHDA) phase or to the contunite crystal likely occurs in ZrO_2 at high pressures. Interestingly these cotunnite-like units in the HDA phase are found to be unquenchable to the ambient pressure in stark contrast to the quenchable cotunnite crystal. Additionally, the formation of cotunnite-like configuration from tetragonal-like topology might imply that a direct phase transformation from the tetragonal crystal to the cotunnite type crystal can be achievable at high temperature and pressure conditions. Additional studies are required to validate or invalidate both speculations.

Finally we need to stress here that due to the some conditions/limitations of simulations such as absence of surface effects because of the use of periodic boundary conditions, fast pressurizing etc., the transformation pressures/starting pressures observed in simulations are generally overestimated. Therefore the starting and ending pressures of the LDA-to-HDA phase transformation in experiments is anticipated to be lower than ones predicted in the simulations.

5 | CONCLUSIONS

We have performed ab initio simulations to examine the high-pressure behavior of *a*-ZrO_2 and discussed, for the first time, a possible amorphous-to-amorphous phase change. The phase change involves a gradual coordination modification of Zr atoms from 6.81 to 8.0 and O atoms from 3.4 to 4.0. Since the crystalline phase having eightfold-coordinated Zr atoms does not form in ZrO_2 under pressure, the phase transformation mechanism of *a*-ZrO_2 is proposed to be different from that of the crystal at high pressure but similar to the one observed at high temperature. The leading packing unit of the dense noncrystalline state is eightfold-coordinated Zr atoms (62.5%) and is comparable to that of high-temperature tetragonal phase. When the applied pressure is fully released, the original structure is not recovered and instead a structural change to another amorphous state is detected. This dense amorphous configuration is structurally intermediate between LDA and HDA phases. During the compression and decompression processes, *a*-ZrO_2 remains semiconductor. Yet the uncompressed model has the largest band gap energy relative to the other dense amorphous states. We also speculate that a phase transformation from the HDA state to the cotunnite-like VHDA state or to the cotunnite crystal likely takes place in ZrO_2 at higher pressures.

ACKNOWLEDGMENTS

This work was supported by the Abdullah Gül University Support Foundation. The calculations were run on TÜBİTAK ULAKBİM, High Performance and Grid Computing Center (TRUBA resources).

ORCID

Murat Durandurdu http://orcid.org/0000-0001-5636-3183

REFERENCES

1. Singhal SC. Zirconia electrolyte based fuel cells. High Temp Mater Proc. 2002;5:43–53.
2. Ishihara T, Sato K, Takita Y. Electrophoretic deposition of Y2O3-stabilized ZrO2 electrolyte films in solid oxide fuel cells. J Am Ceram Soc. 1996;79:913–9.
3. Luo J, Ball RJ, Stevens R. Gadolinia doped ceria/yttria stabilized zirconia electrolytes for solid oxide fuel cell applications. J Mater Sci. 2004;39:235–40.
4. Wu YH, Chen LL, Chen WC, Lin CC, Wu ML, Wu JR. MOS devices with tetragonal ZrO_2 as gate dielectric formed by annealing ZrO_2/Ge/ZrO_2 laminate. Microelectron Eng. 2011;88:1361–4.
5. Panda D, Tseng TY. Growth, dielectric properties, and memory device applications of ZrO_2 thin films. Thin Solid Films. 2013;531:1–20.
6. Lee B, Choi KJ, Hande A, Kim MJ, Wallace RM, Kim J, et al. A novel thermally-stable zirconium amidinate ALD precursor for ZrO_2 thin films. Microelectron Eng. 2009;86:272–6.
7. Manicone PF, Iommetti PR, Raffaelli L. An overview of zirconia ceramics: basic properties and clinical applications. J Dent. 2007;35:819–26.
8. Denry I, Kelly JR. State of the art of zirconia for dental applications. Dent Mater. 2008;24:299–307.
9. Sato AG, Volanti DP, Meira DM, Damyanova S, Longo E, Bueno JM. Effect of the ZrO2 phase on the structure and behavior of supported Cu catalysts for ethanol conversion. J Catal. 2013;307:1–7.

10. Cardarelli F. *Materials handbook*. London, UK: Springer; 2000.
11. Wolten GM. Diffusionless phase transformations in zirconia and hafnia. J Am Ceram Soc. 1963;46:418–22.
12. Aldebert P, Traverse JP. Structure and ionic mobility of zirconia at high temperature. J Am Ceram Soc. 1985;68:34–40.
13. Ishigame M, Sakurai T. Temperature dependence of the Raman spectra of ZrO_2. J Am Ceram Soc. 1977;60:367–9.
14. Kudoh Y, Takeda H, Arashi H. In situ determination of crystal structure for high pressure phase of ZrO2 using a diamond anvil and single crystal X-ray diffraction method. Phys Chem Miner. 1986;13:233–7.
15. Heuer AH, Lanteri V, Farmer SC, Chaim R, Lee RR, Kibbel BW, et al. On the orthorhombic phase in ZrO_2-based alloys. J Mater Sci. 1989;24:124–32.
16. Leger JM, Tomaszewski PE, Atouf A, Pereira AS. Pressure-induced structural phase transitions in zirconia under high pressure. Phys Rev B Condens Matter. 1993;47:14075–83.
17. Desgreniers S, Lagarec K. High-density ZrO_2 and HfO_2: crystalline structures and equations of state. Phys Rev B Condens Matter. 1999;59:8467–72.
18. Haines J, Léger JM, Hull S, Petitet JP, Pereira AS, Perottoni CA, et al. Characterization of the cotunnite-type phases of zirconia and hafnia by neutron diffraction and Raman spectroscopy. J Am Ceram Soc. 1997;80:1910–4.
19. Block S, Jornada JD, Piermarini GJ. Pressure-temperature phase diagram of zirconia. J Am Ceram Soc. 1985;68:497–9.
20. Haines J, Léger JM, Atouf A. Crystal structure and equation of state of cotunnite-type zirconia. J Am Ceram Soc. 1995;78:445–8.
21. Alzyab B, Perry CH, Ingel RP. High-pressure phase transitions in zirconia and yttria-doped zirconia. J Am Ceram Soc. 1987;70:760–5.
22. Arashi H, Yagi T, Akimoto S, Kudoh Y. New high-pressure phase of ZrO_2 above 35 GPa. Phys Rev B Condens Matter. 1990;41:4309–13.
23. Ohtaka O, Yamanaka T, Yagi T. New high-pressure and-temperature phase of ZrO_2 above 1000° C at 20 GPa. Phys Rev B Condens Matter. 1994;49:9295–8.
24. Öztürk H, Durandurdu M. High-pressure phases of ZrO2: an ab initio constant-pressure study. Phys Rev B Condens Matter. 2009;79:134111–6.
25. Al-Khatatbeh Y, Lee KK, Kiefer B. Phase relations and hardness trends of ZrO_2 phases at high pressure. Phys Rev B Condens Matter. 2010;81:214102–21411.
26. Nishio-Hamane D, Dekura H, Seto Y, Yagi T. Theoretical and experimental evidence for the post-cotunnite phase transition in zirconia at high pressure. Phys Chem Miner. 2015;42:385–92.
27. Durandurdu M. Novel high-pressure phase of ZrO_2: an ab initio prediction. J Solid State Chem. 2015;230:233–6.
28. Parreira P, Paterson GW, McVitie S, MacLaren DA. Stability, bistability and instability of amorphous ZrO_2 resistive memory devices. J Phys D Appl Phys. 2016;49:095111–6.
29. Kumar A, Mondal S, Rao KK. Low temperature solution processed high-κ ZrO_2 gate dielectrics for nanoelectonics. Appl Surf Sci. 2016;370:373–9.
30. Ye G, Wang H, Arulkumaran S, Ng GI, Hofstetter R, Li Y, et al. Atomic layer deposition of ZrO_2 as gate dielectrics for AlGaN/GaN metal-insulator-semiconductor high electron mobility transistors on silicon. Appl Phys Lett. 2013;103:142109–11.
31. Chagarov E, Kummel AC. Generation of realistic amorphous Al_2O_3 And ZrO_2 samples by hybrid classical and first-principle molecular dynamics simulations. ECS Trans. 2008;16:773–85.
32. Zhao X, Ceresoli D, Vanderbilt D. Structural, electronic, and dielectric properties of amorphous ZrO_2 from ab initio molecular dynamics. Phys Rev B Condens Matter. 2005;71:085107–16.
33. Vanderbilt D, Zhao X, Ceresoli D. Structural and dielectric properties of crystalline and amorphous ZrO_2. Thin Solid Films. 2005;486:125–8.
34. Durandurdu M. Amorphous zirconia: ab initio molecular dynamics simulations. Philos Mag. 2017;97:1334–45.
35. Kurapova OY, Konakov VG. Phase evolution in zirconia based systems. Rev Adv Mater Sci. 2014;36:177–90.
36. Pavlik RS, Klein LC, McCauley RA. Experimental design applied to the chemical durability of sol–gel-derived zirconias. J Am Ceram Soc. 1997;80:1469–76.
37. Sayan S, Nguyen NV, Ehrstein J, Emge T, Garfunkel E, Croft M, et al. Structural, electronic, and dielectric properties of ultrathin zirconia films on silicon. Appl Phys Lett. 2005;86:152902–4.
38. Ordejon P, Artacho E, Soler JM. Self-consistent order-N density-functional calculations for very large systems. Phys Rev B Condens Matter. 1996;53:R10441–4.
39. Troullier N, Martins JL. Efficient pseudopotentials for plane-wave calculations. Phys Rev B Condens Matter. 1991;43:1993–2006.
40. Perdew JP, Burke K, Ernzerhof M. Generalized gradient approximation made simple. Phys Rev Lett. 1996;77:3865–8.
41. Parrinello M, Rahman A. Polymorphic transitions in single crystals: a new molecular dynamics method. J Appl Phys. 1981;52:7182–90.
42. Medvedev NN. The algorithm for three-dimensional voronoi polyhedra. J Comput Phys. 1986;67:223–9.
43. Gritsenko V, Gritsenko D, Shaimeev S, Aliev V, Nasyrov K, Erenburg S, et al. Atomic and electronic structures of amorphous ZrO_2 and HfO_2 films. Microelectron Eng. 2005;81:524–9.

How to cite this article: Durandurdu M. Amorphous zirconia at high pressure. *J Am Ceram Soc*. 2018;00:1–8. https://doi.org/10.1111/jace.15805